

Diffuse Interstellar Bands vs. Known Atomic and Molecular Species in the Interstellar Medium of M82 toward SN 2014J

Daniel E. Welty¹, Adam M. Ritchey², Julie A. Dahlstrom³, Donald G. York^{1,4}

ABSTRACT

We discuss the absorption due to various constituents of the interstellar medium of M82 seen in moderately high resolution, high signal-to-noise ratio optical spectra of SN 2014J. Complex absorption from M82 is seen, at velocities $45 \lesssim v_{\text{LSR}} \lesssim 260 \text{ km s}^{-1}$, for Na I, K I, Ca I, Ca II, CH, CH⁺, and CN; many of the diffuse interstellar bands (DIBs) are also detected. Comparisons of the column densities of the atomic and molecular species and the equivalent widths of the DIBs reveal both similarities and differences in relative abundances, compared to trends seen in the ISM of our Galaxy and the Magellanic Clouds. Of the ten relatively strong DIBs considered here, six (including $\lambda 5780.5$) have strengths within $\pm 20\%$ of the mean values seen in the local Galactic ISM, for comparable $N(\text{K I})$; two are weaker by 20–45% and two (including $\lambda 5797.1$) are stronger by 25–40%. Weaker than “expected” DIBs [relative to $N(\text{K I})$, $N(\text{Na I})$, and $E(B - V)$] in some Galactic sight lines and toward several other extragalactic supernovae appear to be associated with strong CN absorption and/or significant molecular fractions. While the $N(\text{CH})/N(\text{K I})$ and $N(\text{CN})/N(\text{CH})$ ratios seen toward SN 2014J are similar to those found in the local Galactic ISM, the combination of high $N(\text{CH}^+)/N(\text{CH})$ and high $W(5797.1)/W(5780.5)$ ratios has not been seen elsewhere. The centroids of many of the M82 DIBs are shifted, relative to the envelope of the K I profile – likely due to component-to-component variations in $W(\text{DIB})/N(\text{K I})$ that may reflect the molecular content of the individual components. We compare estimates for the host galaxy reddening $E(B - V)$ derived from the various interstellar species with the values estimated from optical and near-IR photometry of SN 2014J.

Subject headings: galaxies: individual (M82), galaxies: ISM, ISM: atoms, ISM: lines and bands, ISM: molecules, supernovae: individual (SN 2014J)

¹University of Chicago, Department of Astronomy and Astrophysics, 5640 S. Ellis Ave., Chicago, IL 60637; dwelty@oddjob.uchicago.edu

²University of Washington, Department of Astronomy, Box 351580, Seattle, WA 98195

³Carthage College, Department of Physics and Astronomy, 2001 Alford Park Dr., Kenosha, WI 53140

⁴also, Enrico Fermi Institute

1. INTRODUCTION

Supernovae in external galaxies provide rare, fleeting opportunities to probe the interstellar media of the host galaxies via absorption-line spectroscopy. In principle, such observations can reveal the behavior of various tracers of the ISM under somewhat different environmental conditions from those typically sampled in the local Galactic ISM. Differences in overall metallicity, specific elemental abundance ratios, dust-to-gas ratios, and radiation fields all can affect the structure and composition of interstellar clouds (e.g., Wolfire et al. 1995; Pak et al. 1998); in combination, the overall effects can be somewhat unexpected and counter-intuitive. Exploration of diverse environments, where those factors act in different combinations, thus can aid in disentangling the specific effects of each factor.

It is particularly important to compare the behavior of the enigmatic diffuse interstellar bands (DIBs) in a variety of environments with the corresponding behavior of known atomic and molecular constituents of the ISM. Such comparisons should aid both in identifying the carriers of the DIBs and in calibrating the DIBs as diagnostics of the physical conditions in the ISM. Some of the typically strongest DIBs (in the local Galactic ISM) have therefore been measured toward a small number of stars in the Large and Small Magellanic Clouds (LMC and SMC; Vladilo et al. 1987; Ehrenfreund et al. 2002; Cox et al. 2006, 2007; Welty et al. 2006), toward a much larger set of stars in the 30 Dor region of the LMC (van Loon et al. 2013), and toward some stars in M33 (Cordiner et al. 2008b) and M31 (Cordiner et al. 2008a, 2011). A few DIBs have been detected in the host galaxies of extragalactic supernovae (D’Odorico et al. 1989; Sollerman et al. 2005; Cox & Patat 2008, 2014) and in several damped Lyman- α systems (York et al. 2006; Ellison et al. 2008; Lawton et al. 2008); Phillips et al. (2013) have compiled measurements of the $\lambda 5780.5$ DIB toward a number of recent Type Ia SNe. Examination of the behavior of the DIBs in the Local Group galaxies suggests that the DIB strengths can depend both on the overall metallicity and on local physical conditions (e.g., radiation field, molecular fraction). Certain DIB ratios (e.g., $\lambda 5797.1/\lambda 5780.5$) may provide information on the ambient radiation fields (e.g., Vos et al. 2011); the strengths of individual DIBs (e.g., $\lambda 5780.5$) may yield useful estimates for the color excess $E(B - V)$ and the column density of atomic hydrogen $N(\text{H})$ where those quantities cannot be directly determined (e.g., Herbig 1993; Friedman et al. 2011; Phillips et al. 2013).

The discovery of SN 2014J in M82 (Fossey et al. 2014) provided an opportunity to obtain moderately high resolution, high signal-to-noise (S/N) ratio spectra of a bright, nearby supernova at multiple epochs (both before and after maximum apparent brightness) – enabling searches for weak interstellar features and for temporal variations in the absorption that might reveal changes in circumstellar material (e.g., Patat et al. 2007; Sternberg et al. 2011, 2013). As summarized by Goobar et al. (2014), analyses of the early photometry and optical spectra suggest that SN 2014J is a Type Ia, significantly reddened by intervening interstellar material located primarily within M82; estimates of $E(B - V)$ range from about 0.8 to 1.2 mag. Absorption from a number of known interstellar species and from many DIBs in M82 thus might be detectable in high-S/N ratio spectra of the supernova. Unfortunately, Type Ia SNe typically have very little UV flux below about 2600

Å (e.g., Foley & Kirshner 2011), making UV spectra impractical to obtain – so that investigations of the intervening ISM will have to depend largely on interpreting the species observable in the optical and infrared.

In this paper, we discuss the interstellar absorption features seen in multi-epoch, moderately high resolution, high-S/N ratio optical spectra obtained with the ARC echelle spectrograph (ARCES; Wang et al. 2003) at Apache Point Observatory (APO). Section 2 describes the observations and the processing of the raw spectral images. Section 3 presents the observed interstellar features, with some comparison to those seen toward several other SNe. Section 4 discusses some of the atomic and molecular species and several of the DIBs – in the context of trends observed in the ISM of our Galaxy, the LMC, and the SMC – yielding some insights into the behavior of the DIBs and the properties of the M82 ISM toward SN 2014J. Section 5 summarizes our results and conclusions. Two companion papers focus on the abundances and kinematics of the observed atomic and molecular species (Ritchey et al. 2014b) and on a more complete census of the DIBs detected toward SN 2014J (York et al. 2014).

2. OBSERVATIONS AND DATA ANALYSIS

Forty-seven 20-minute exposures of SN 2014J were obtained with ARCES on six nights (2014 January 27, 30; February 08, 11, 22; March 04) – i.e., both before and after the observed peak in V-band brightness of the SN around 2014 February 02. With the currently installed echelle grating, the spectra cover nearly the full optical range from about 3800 to 11000 Å at a resolution of about 31,500 (slightly lower than with the previous grating). Independent reductions of the individual raw spectral images, employing standard procedures for ARCES spectra (e.g., Thorburn et al. 2003), were performed by AR and JD. Minor differences in the extracted spectra for any given individual exposure may be attributed to slight differences employed in removing cosmic ray events. The 5–13 individual spectra obtained on each night were corrected for telluric absorption features (via observations of bright, lightly-reddened standard stars), shifted to a common velocity scale (local standard of rest), and co-added to produce nightly sum spectra. Because no significant changes were noted in the absorption-line profiles (Ritchey et al. 2014b), a total sum of all 47 spectra was also constructed (though only the 29 spectra from the first four nights were used below about 4500 Å, due to the significantly lower flux in the blue on the last two nights).

Spectral segments around the various interstellar absorption features of interest were normalized via low-order polynomial fits to adjacent continuum regions. The nightly sum spectra have S/N ratios of order 300–400 (per resolution element) near 6000 Å, and of order 100 below 4000 Å, as determined from the scatter in the continuum fits. Equivalent widths and apparent optical depth (AOD) estimates for the column densities of known atomic and molecular species and equivalent widths for the DIBs were then measured from the normalized spectra. Where possible, separate values were measured for the absorption from our Galaxy and from M82, taking $v_{\text{LSR}} = 30 \text{ km s}^{-1}$ as the dividing line. For the DIBs, the ranges over which the equivalent widths were

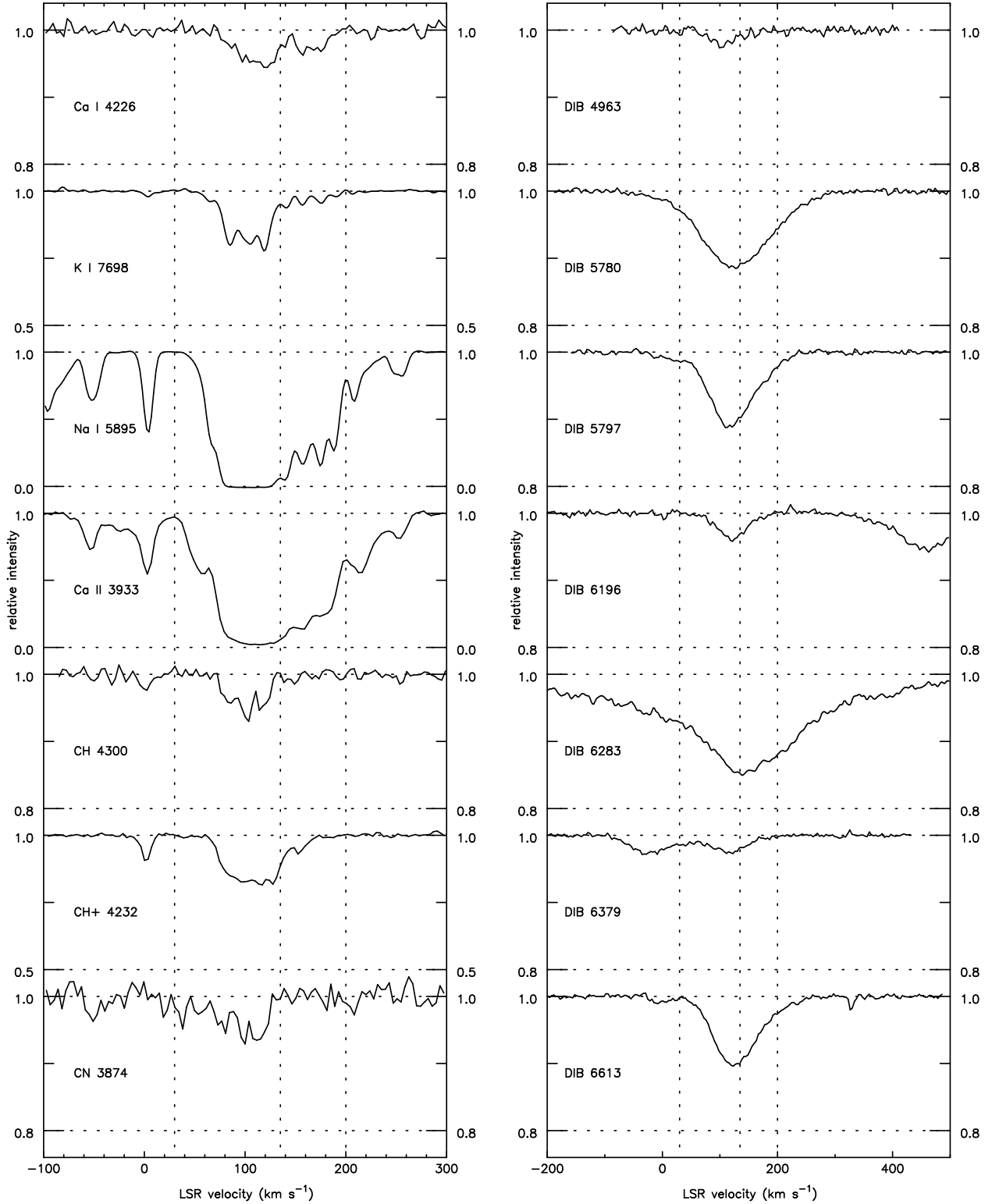


Fig. 1.— ARCES spectra of interstellar atomic and molecular absorption lines (left) and selected diffuse interstellar bands (right) toward SN 2014J. Dotted vertical lines separate three groups of K I components: the Galactic components (at $v_{\text{LSR}} \lesssim 30 \text{ km s}^{-1}$), the stronger “main” M82 components between 85 and 120 km s^{-1} and the weaker, higher velocity M82 components between 125 and 190 km s^{-1} . Still weaker M82 components are seen in Na I and Ca II. The absorption between about 10 and 60 km s^{-1} for CN is for the CN R1 line.

measured are consistent with those adopted by Friedman et al. (2011; see their figure 1), with allowance for broadening of the features due to the complex component structure observed for the material in M82. The uncertainties in the measured equivalent widths include contributions from photon noise, continuum placement, and the range in values found for different combinations of the two independently reduced sets of spectra. Independent multi-component fits to the profiles of the atomic and molecular lines were performed, using the codes **ismod** (AR; see Sheffer et al. 2008) and **fits6p** (DW; see Welty et al. 2003), to obtain estimates for column densities, line widths, and velocities for the "individual" components discernible in the spectra (Ritchey et al. 2014b).

3. RESULTS

Absorption from Na I, K I, Ca I, Ca II, CH, CH⁺, CN, and many of the DIBs is clearly visible in the summed, normalized spectra of SN 2014J (Fig. 1). The atomic and molecular lines exhibit multiple components, at LSR velocities ranging from about -53 to $+257$ km s⁻¹ (Cox et al. 2014; Goobar et al. 2014; Ritchey et al. 2014a, 2014b). Examination of the available 21 cm emission profiles in the region around M82 (e.g., Kalberla et al. 2005) suggests that the components at $v_{\text{LSR}} \lesssim 30$ km s⁻¹ are due to gas in the Galactic disk and halo, with total $N(\text{H}) \sim 3.65 \times 10^{20}$ cm⁻², while components at higher velocities are due to gas associated with M82. For K I and CH, the weak absorption near $v_{\text{LSR}} = 0$ km s⁻¹ is due to the main Galactic disk component (seen more strongly in Na I and Ca II); several relatively strong components from about 85 to 120 km s⁻¹ (saturated in Na I) and weaker components from about 65 to 80 and 125 to 190 km s⁻¹ arise in M82; additional components, at both lower and higher velocities, are visible in the stronger lines of Na I and Ca II (Ritchey et al. 2014b). That complex structure is not directly discernible in the intrinsically broader DIBs, where the contributions from the individual components seen in K I overlap and blend together to produce relatively smooth, broad absorption features (though see Sec. 4.3 below).

While many DIBs are detected toward SN 2014J (York et al. 2014), we focus in this paper on a subset of ten (Table 1): the eight relatively strong DIBs examined by Friedman et al. (2011), the $\lambda 6379.3$ DIB, and the $\lambda 4963.9$ "C₂-DIB" (Thorburn et al. 2003), for which significant sets of uniformly measured Galactic data are available for comparison. The relatively small velocity difference between the Galactic and M82 absorption toward SN 2014J means that contributions from the two galaxies will be blended for the intrinsically broader DIBs. The Galactic contributions to the measured total equivalent widths of those broader DIBs may be estimated via the observed Galactic column densities of K I and atomic hydrogen and the mean relationships between those neutral atomic species and the DIBs found in the Galactic ISM (column 4 of the table; see Friedman et al. 2011 and the Appendix to this paper). Comparisons with the Galactic equivalent widths measured for several of the narrower DIBs and with the residuals from crude fits to the profiles of several of the broader DIBs (which included only M82 components; see Sec. 4.3 below) in column 5, however, suggest that those estimated Galactic contributions are a factor of ~ 2 too large. Our

Table 1. M82 DIBs and Predicted $E(B - V)$

DIB	FWHM ^a (Å)	$W(\text{total})$ (meas)	$W(\text{MW})^b$ (pred H/K I)	$W(\text{MW})^c$ (meas)	$W(\text{MW})^d$ (adopt)	$W(\text{M82})^e$ (diff)	$W(\text{M82})^f$ (pred)	$E(B - V)^g$ (pred)	$E(B - V)^h$ (corr)
(1)	(2)	(3)	(4)	(5)	(6)	(7)	(8)	(9)	(10)
4963.9	0.62	23±3	2/1	...	(1)	23±3	22	0.74	0.70
5487.7	5.20	96±13	14/14	...	7±4	89±13	75	0.79	0.70
5705.1	2.58	61±7	12/13	...	6±3	55±8	71	0.48	0.59
5780.5	2.11	343±13	46/50	18±3	24±12	319±18	346	0.62	0.66
5797.1	0.77	218±4	14/16	7±2	8±4	210±6	151	1.18	0.96
6196.0	0.42	46±5	5/5	2±1	(2)	46±5	40	0.92	0.84
6203.6	4.87	162±13	24/24	...	12±6	150±14	130	0.83	0.74
6283.8	4.77	956±16	173/188	...	90±45	866±48	906	0.75	0.77
6379.3	0.58	41±4	6/5	...	(3)	41±4	73	0.43	0.64
6613.6	0.93	226±5	10/10	<9	(5)	226±5	176	1.07	0.93
average								0.78±0.24	0.75±0.12

^aFWHM measured toward HD204827 (Hobbs et al. 2009).

^bPredicted $W(\text{DIB})$ for Milky Way, assuming $\log[N(\text{H})] = 20.56$ and Galactic relationships from Friedman et al. (2011) and assuming $\log[N(\text{K I})] = 10.53$ and Galactic relationships given in Appendix Table 3.

^cMeasured $W(\text{DIB})$ for Milky Way, for narrower DIBs.

^dAdopted $W(\text{DIB})$ for Milky Way: $0.5 \times$ the predicted values, with $\pm 50\%$ assumed uncertainty.

^e $W(\text{DIB})$ for M82: measured total minus adopted Galactic, for broader DIBs only.

^fPredicted $W(\text{DIB})$ for M82, assuming $\log[N(\text{K I})] = 12.28$ and Galactic relationships given in Appendix Table 3.

^gPredicted M82 $E(B - V)$ from M82 $W(\text{DIB})$ and Galactic relationships from Friedman et al. (2011).

^hPredicted M82 $E(B - V)$, adjusted for residuals [$W(\text{M82})$ minus $W(\text{pred})$], using relationships given in Appendix Table 3.

adopted estimates for the Galactic contributions to the DIBs, with assumed $\pm 50\%$ uncertainties, are given in column 6 of the table; those uncertainties are included in the uncertainties listed for the derived host galaxy equivalent widths in column 7.

Table 2 compares the host galaxy column densities for the atomic and molecular species and the host galaxy equivalent widths for the ten selected DIBs found toward SN 2014J with those found toward four other extragalactic SNe and in three Galactic sight lines. Of the four other extragalactic sight lines listed in columns 3–6 of the table, those toward SN 1986G (NGC 5128; D’Odorico et al. 1989), SN 2006X (M100; Lauroesch et al. 2006; Patat et al. 2007; Cox & Patat 2008), and SN 2008fp (ESO428-G14; Cox & Patat 2014) also exhibit absorption from CH, CH⁺, and/or CN. The values for the host galaxy A_V and R_V listed by Phillips et al. (2013) imply corresponding host galaxy $E(B - V) \sim 0.8$, 1.4, and 0.6, respectively, toward those three SNe. No molecular absorption was detected toward SN 2001el (NGC 1448; Sollerman et al. 2005; this paper), but relatively strong absorption from Na I and Ca II and measurable absorption from a number of DIBs have been noted; the estimated $E(B - V)$ is 0.28.

The column densities, equivalent widths, and ratios found toward the three Galactic stars are given in columns 7–9 of Table 2. The sight line toward HD62542 is dominated by a single cloud with high molecular fraction (Snow et al. 2002; Ádámkóvics et al. 2005). The sight lines toward the two DIB atlas stars HD183143 and HD204827 exhibit distinctly different relative molecular abundances and DIB strengths (Thorburn et al. 2003; Hobbs et al. 2008, 2009), and may have comparable $E(B - V)$ to SN 2014J. The high abundances of CN, C₂, and C₃ toward HD 62542 and HD204827 suggest that the densities and molecular fractions are high in the main clouds in those sight lines; the lower $N(\text{CN})/N(\text{CH})$ and higher $N(\text{CH}^+)/N(\text{CH})$ ratios toward HD183143 suggest that the clouds there are more diffuse. Toward HD183143, nine of the ten DIBs listed in the table lie on or above the general Galactic trends versus $E(B - V)$ and $N(\text{K I})$; toward HD204827, nine of the ten DIBs lie on or below those general trends, with only the $\lambda 4963.9$ C₂-DIB stronger than average. The much lower $W(5797.1)/W(5780.5)$ ratio toward HD183143 suggests that the clouds in that sight line are exposed to stronger radiation fields and/or that the DIBs are less shielded (e.g., Vos et al. 2011). The last column of the table gives average Galactic values of the various quantities, for sight lines with $E(B - V) \sim 1.0$.

Table 2. Column Densities, DIB Equivalent Widths, and Ratios toward Five SNe and Three Galactic Stars

Quantity	2014J ^a	1986G	2006X	2008fp	2001el	HD62542	HD183143	HD204827	MW avg
(1)	M82	NGC5128	M100	ESO428-G14	NGC1448	MW	MW	MW	(10)
(1)	(2)	(3)	(4)	(5)	(6)	(7)	(8)	(9)	(10)
$E(B - V)^b$	1.0±0.2	0.79±0.08	1.44±0.13	0.59±0.12	0.28±0.06	0.35±0.03	1.27±0.06	1.11±0.06	(1.00)
$\log[N(\text{Na I})]$	14.2±0.1	13.74	13.8–14.3	14.43±0.03	12.76±0.03	13.93±0.05	14.28±0.03	14.7±0.1	14.59
$\log[N(\text{K I})]$	12.28±0.02	...	12.00±0.04	12.03±0.03	11.29±0.05	11.90±0.18	12.21±0.02	12.81±0.03	12.57
$\log[N(\text{Ca I})]$	11.28±0.07	...	10.8±0.2	11.35±0.02	[10.21±0.11]	<9.37	10.56±0.02	10.58±0.02	10.68
$\log[N(\text{Ca II})]$	13.8±0.1	13.32	[13.24±0.08]	13.39±0.02	12.79±0.08	11.96±0.0x	...	>12.59	...
$\log[N(\text{CN})]$	13.0±0.1	...	14.15±0.15	[13.6±0.1]	[<12.05]	13.62±0.16	12.57±0.02	13.74±0.04	...
$\log[N(\text{CH})]$	13.66±0.04	[13.5±0.1]	13.78±0.03	13.45±0.36	[<12.68]	13.54±0.02	13.67±0.03	13.90±0.04	13.77
$\log[N(\text{CH}^+)]$	14.33±0.02	[13.6±0.1]	13.65±0.10	13.23±0.22	[<12.66]	<11.84	13.83±0.02	13.57±0.04	13.76
$W(4963.9)$	23±3	...	[8±5]	...	[7±4]	6±1	26±1	53±1	29
$W(5487.7)$	89±13	225±14	68±4	123
$W(5705.1)$	55±8	79±5	37±5	...	172±7	58±3	114
$W(5780.5)$	319±18	335±5	<72	81±5	189±3	31±6	761±6	257±4	490
$W(5797.1)$	210±6	151±5	...	60±10	26±2	12±2	257±8	199±3	195
$W(6196.0)$	46±5	30±15	14±4	29±6	15±2	3±1	89±2	42±1	54
$W(6203.6)$	150±14	191±5	[47±15]	[48±9]	102±5	15±4	340±11	116±4	197
$W(6283.8)$	866±48	...	177±25	180±30	500±80	50±20	1910±30	518±60	1217
$W(6379.3)$	41±4	(75±8)	<8	[17±3]	12±3	...	105±1	95±1	87
$W(6613.6)$	226±5	...	<18	...	52±3	8±1	332±4	171±3	241
$\log[N(\text{Ca I})/N(\text{K I})]$	-1.00±0.07	...	-1.2±0.2	-0.68±0.04	-1.08±0.12	< -2.53	-1.65±0.03	-2.23±0.04	-2.05
$\log[N(\text{CH})/N(\text{K I})]$	+1.38±0.04	...	+1.78±0.05	+1.42±0.36	<+1.39	+1.64±0.18	+1.46±0.04	+1.09±0.05	+1.26
$\log[N(\text{CN})/N(\text{CH})]$	-0.66±0.11	...	+0.37±0.15	+0.15±0.37	...	+0.08±0.16	-1.10±0.04	-0.16±0.06	...
$\log[N(\text{CH}^+)/N(\text{CH})]$	+0.67±0.04	+0.10±0.14	-0.13±0.10	-0.22±0.42	...	< -1.70	+0.16±0.04	-0.33±0.06	...
$W(5797.1)/W(5780.5)$	0.66±0.04	0.45±0.02	...	0.74±0.13	0.14±0.01	0.39±0.10	0.34±0.01	0.77±0.02	0.41
$10^5 W(4963.9)/[N(\text{K I})]^{1/2}$	1.7±0.2	...	0.8±0.5	...	1.6±0.9	0.7±0.2	2.0±0.1	2.1±0.1	1.8
$10^5 W(5780.5)/[N(\text{K I})]^{1/2}$	23.1±1.4	...	<7.2	7.8±0.6	42.8±2.6	3.5±1.0	59.8±1.5	10.1±0.4	33.9
$10^5 W(5797.1)/[N(\text{K I})]^{1/2}$	15.2±0.6	5.8±1.0	5.9±0.6	1.3±0.4	20.2±0.8	7.8±0.3	13.0
$10^5 W(6196.0)/[N(\text{K I})]^{1/2}$	3.3±0.4	...	1.4±0.4	2.8±0.6	3.4±0.5	0.3±0.1	7.0±0.2	1.7±0.1	3.7
$10^5 W(6283.8)/[N(\text{K I})]^{1/2}$	62.7±3.8	...	17.7±2.6	17.4±3.0	113.2±19.3	5.6±2.5	150.0±4.2	20.4±2.5	93.3
$W(4963.9)/E(B - V)$	23±5	...	6±4	...	25±15	17±3	20±1	48±3	25
$W(5780.5)/E(B - V)$	319±66	424±43	<50	137±29	675±145	89±19	599±29	232±13	463
$W(5797.1)/E(B - V)$	210±42	191±20	...	102±27	93±21	34±6	202±11	179±10	182
$W(6196.0)/E(B - V)$	46±11	38±19	10±3	49±14	54±14	9±3	70±4	38±3	52
$W(6283.8)/E(B - V)$	866±180	...	123±21	305±80	1786±478	143±58	1504±75	467±60	1151

4. DISCUSSION

4.1. Trends in the Milky Way and Magellanic Clouds

In the local Galactic ISM, a number of fairly well defined trends may be noted (pairwise) between the column densities of Na I, K I, H, and H₂, the equivalent widths of various DIBs, and $E(B - V)$ (Herbig 1993; Welty & Hobbs 2001; Friedman et al. 2011). Unusual environmental conditions characterizing particular regions or individual sight lines may account for observed deviations from those general trends. For example, the column densities of the trace neutral species K I and Na I exhibit nearly quadratic relationships with the total hydrogen column density $N(\text{H}_{\text{tot}}) = N(\text{H}) + 2N(\text{H}_2)$ and with $E(B - V)$ (left-hand panel of Fig. 2) – consistent with considerations of ionization equilibrium – and roughly linear relationships with $N(\text{H}_2)$ [for $N(\text{H}_2) > 10^{18} \text{ cm}^{-2}$] (Welty & Hobbs 2001)¹. The DIBs, on the other hand, appear to exhibit roughly linear relationships with $N(\text{H})$, $N(\text{H}_{\text{tot}})$, and $E(B - V)$ (right-hand panel of Fig. 2), and roughly square-root relationships with $N(\text{Na I})$ and $N(\text{K I})$ (i.e., slopes ~ 0.5 in log-log plots; Fig. 3); for most DIBs, there is no residual or secondary correlation with $N(\text{H}_2)$ (Herbig 1993; Welty et al. 2006; Friedman et al. 2011; Welty 2014). [Note that the DIBs generally appear to be unsaturated – at least for $W(5780.5) \lesssim 800 \text{ m\AA}$ (e.g., Thorburn et al. 2003) – so that their equivalent widths are linearly related to the abundances of the carrier molecules and may be directly compared with the column densities of the atomic and molecular species.] These general Galactic relationships motivate the ratios given in the lower part of Table 2 – $W(\text{DIB})/E(B - V)$ and $W(\text{DIB})/[N(\text{K I})]^{1/2}$ – which can facilitate the comparisons of DIB strengths in different sight lines. In this paper, we focus on comparisons between the DIBs and K I, as it can be difficult to gauge potential saturation effects on the strong Na I $\lambda\lambda 5890.0, 5895.9$ lines in the moderate-resolution, modest S/N ratio spectra typically available for extragalactic targets – which can make it difficult to determine accurate Na I column densities.²

Examination of the "outlier" sight lines in such correlation plots enables exploration of the effects of local physical conditions on the strengths of various interstellar species. Lower than expected values for $N(\text{Na I})$, $N(\text{K I})$, and the equivalent widths of some DIBs, relative to $N(\text{H}_{\text{tot}})$, in the Sco-Oph and (especially) the Orion Trapezium regions may be due to enhanced radiation fields. Many of the typically stronger, well-studied "standard" DIBs (e.g., $\lambda 5780.5$) can also be

¹Unless otherwise stated, column densities for Galactic and Magellanic Clouds sight lines used in the correlation plots are from online compilations maintained at <http://astro.uchicago.edu/~dwelty/coldens.html> and [coldens_mc.html](http://astro.uchicago.edu/~dwelty/coldens_mc.html), where references to the sources of the data may also be found.

²We note that unrecognized saturation effects in the Galactic Na I data tabulated by Welsh et al. (2010) and used by Phillips et al. (2013) to define fiducial Galactic relationships appear to have biased the slopes of those fiducial relationships. The slopes for Galactic $N(\text{Na I})$ and $N(\text{K I})$ versus A_V (assumed to be the same) are thus underestimated (~ 1.1 vs. ~ 1.8 – 2.0), and the slope for $W(5780.5)$ versus $N(\text{Na I})$ is overestimated (~ 0.9 vs. ~ 0.5) there. Correction of the fiducial relationships for those biases may affect the characterization of sight lines toward some extragalactic SNe as having "anomalously strong" Na I.

Table 2—Continued

Quantity	2014J ^a	1986G	2006X	2008fp	2001el	HD62542	HD183143	HD204827	MW avg
(1)	M82 (2)	NGC5128 (3)	M100 (4)	ESO428-G14 (5)	NGC1448 (6)	MW (7)	MW (8)	MW (9)	(10)

References. — 2014J (this study); 1986G (D’Odorico et al. 1989); 2006X (Patat et al. 2007; Cox & Patat 2008; Phillips et al. 2013); 2008fp (Cox & Patat 2014); 2001el (Sollerman et al. 2005); HD62542 (Ádámkovics et al. 2005; Welty et al., in preparation); HD183143 (Friedman et al. 2011; Hobbs et al. 2009); HD204827 (Friedman et al. 2011; Hobbs et al. 2008); values in square braces were derived for this paper from archival spectra and/or quoted equivalent widths.

^aEstimated Galactic contributions have been removed from measured total DIB equivalent widths: 5487.7 (7 ± 4 mÅ), 5705.1 (6 ± 3 mÅ), 5780.5 (24 ± 12 mÅ), 5797.1 (8 ± 4 mÅ), 6203.6 (12 ± 6 mÅ), 6283.8 (90 ± 45 mÅ); see Table 1.

^b $E(B - V)$ for SN 2014J is from Kotak et al. (2014) and Goobar et al. (2014); values for other SNe are derived from the A_V and R_V tabulated by Phillips et al. (2013).

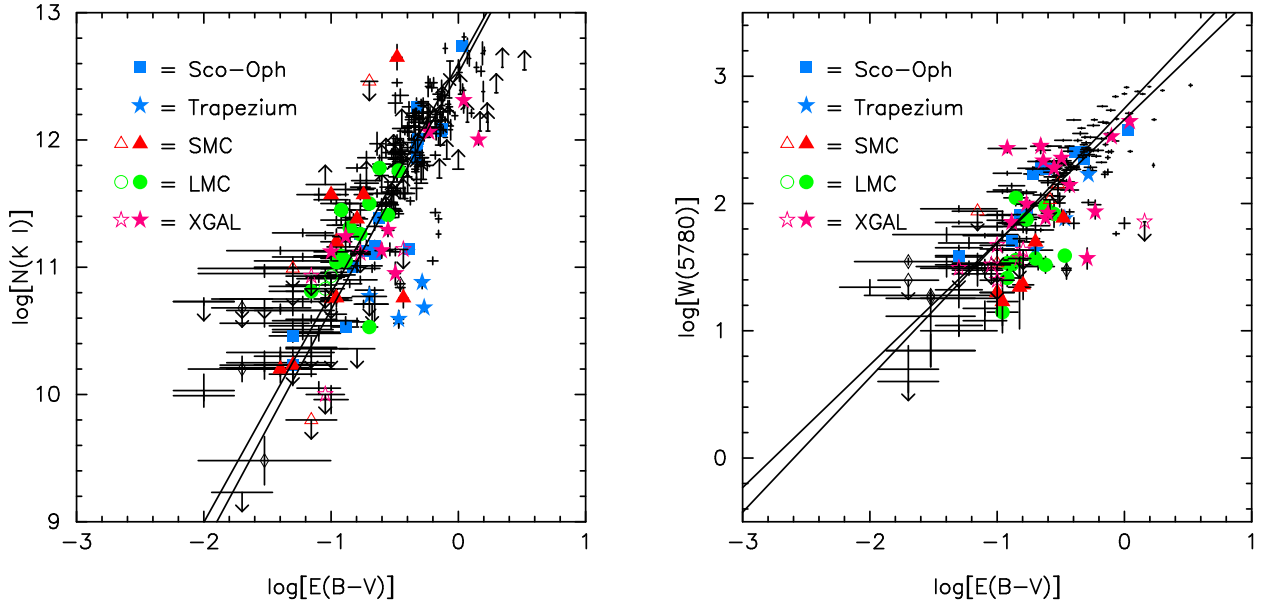


Fig. 2.— $N(\text{K I})$ and $W(5780.5)$ versus $E(B - V)$, for both Galactic and extragalactic sight lines. Solid symbols for LMC, SMC, and extragalactic (XGAL) sight lines denote detections; open symbols denote limits. The Galactic data (plain black crosses) are mostly from Welty & Hobbs (2001) and Friedman et al. (2011). Extragalactic sight lines include quasar absorption-line systems, M31, M33, and external galaxies probed by SNe (mostly from Phillips et al. 2013; see text for other references). The solid lines show weighted and unweighted fits to the Galactic sight lines (not including the Sco-Oph and Trapezium sight lines). The relationship for K I is nearly quadratic (slope ~ 1.8 – 1.9); the relationship for the $\lambda 5780.5$ DIB is roughly linear (slope ~ 1.0). Some sight lines with lower than typical $N(\text{K I})$ have enhanced radiation fields; most of the sight lines with lower than typical $W(5780.5)$ have strong CN and/or higher molecular fractions.

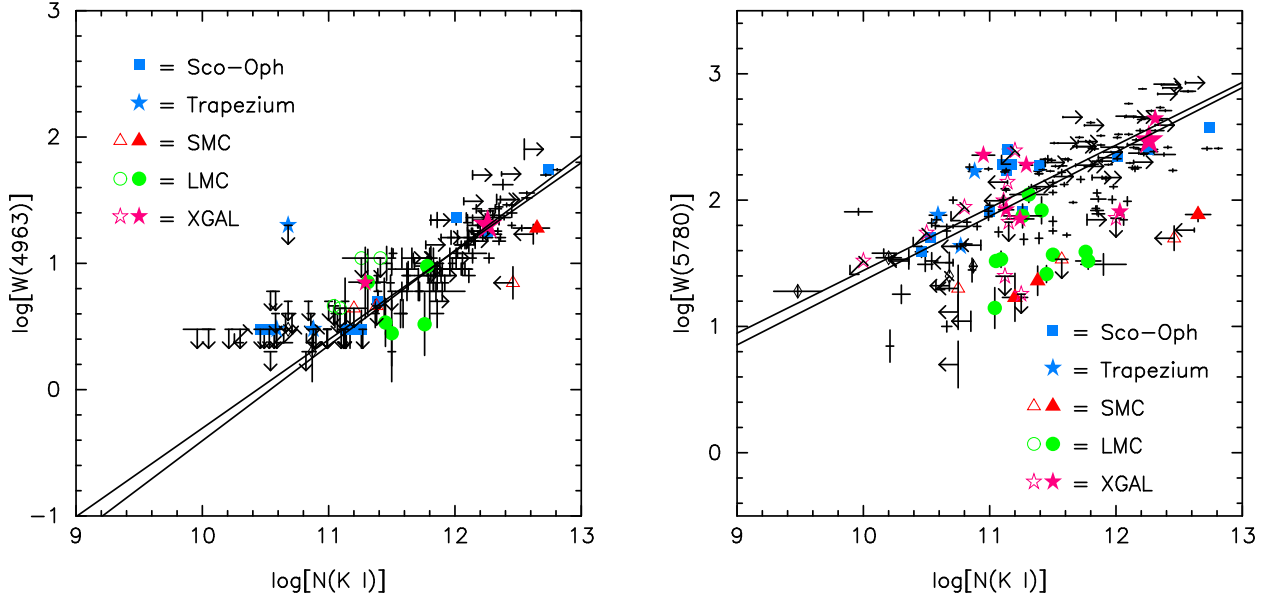


Fig. 3.— Equivalent widths of $\lambda 4963.9$ and $\lambda 5780.5$ DIBs versus $N(\text{K I})$, for both Galactic and extragalactic sight lines. Solid symbols for LMC, SMC, and extragalactic (XGAL) sight lines denote detections; open symbols denote limits. The Galactic data (plain black crosses) are mostly from Welty & Hobbs (2001), Thorburn et al. (2003), and Friedman et al. (2011); the extragalactic data are mostly from Phillips et al. (2013). The solid lines show weighted and unweighted fits to the Galactic sight lines (not including the Sco-Oph and Trapezium sight lines). The relationship for the $\lambda 4963.9$ DIB (a C_2 -DIB) is steeper (slope ~ 0.7), with less scatter, than the relationship for the $\lambda 5780.5$ DIB (slope ~ 0.5). The larger scatter for the $\lambda 5780.5$ DIB may be related to variations in metallicity and/or molecular fraction; detailed comparisons indicate that sight lines deficient in $\lambda 5780.5$ vs. K I tend also to be deficient vs. $E(B - V)$ (see Figs 2 and 4). The M82 gas toward SN 2014J (larger XGAL star near $\log[N(\text{K I})] = 12.3$) lies slightly below the general Galactic trend for $\lambda 5780.5$.

weaker than expected, relative to $N(\text{H}_{\text{tot}})$, $N(\text{Na I})$, $N(\text{K I})$, and $E(B - V)$, in sight lines with strong CN absorption and/or high molecular fractions $f(\text{H}_2) = 2N(\text{H}_2)/N(\text{H}_{\text{tot}})$ (e.g., X Per, HD204827; right-hand panels of Figs. 2 and 3). Those DIBs generally are not weak, relative to $N(\text{H})$, in those sight lines, however. A plot of the residuals of the observed $W(5780.5)$ versus the mean Galactic trends with both $N(\text{K I})$ and $E(B - V)$ (left panel of Figure 4, for the sight line sample of Friedman et al. 2011) shows that sight lines with weak (strong) $W(\lambda 5780.5)$ versus $N(\text{K I})$ thus tend also to have weak (strong) $W(\lambda 5780.5)$ versus $E(B - V)$. The scatter in the residuals plot likely reflects the different processes affecting the trace neutral species (ionization, depletion) and the DIB carriers (ionization, dissociation, depletion, hydrogenation, ...) in different sight lines. Consideration of a few sight lines with even higher molecular abundances (e.g., HD29647, Walker 67, HD62542, NGC2024-1; right panel of Fig. 4) suggests that the relationship between the residuals could be somewhat steeper. Similar relationships between the residuals are seen for the other DIBs in Tables 1 and 2 – particularly for the broader DIBs (see Appendix Table 3). As exemplified by $\lambda 4963.9$ (Thorburn et al. 2003), however, the C_2 -DIBs have somewhat steeper slopes, relative to $N(\text{Na I})$ and $N(\text{K I})$, have weak positive correlations with $f(\text{H}_2)$, and thus are not weaker than expected in sight lines with higher $f(\text{H}_2)$ (left-hand panel of Fig. 3; Welty 2014). The sight line toward HD62542 is an extreme example – with very weak standard DIBs but fairly normal C_2 -DIBs (Snow et al. 2002; Ádámkóvics et al. 2005). The standard DIBs thus appear to trace primarily atomic gas, while the generally weaker C_2 -DIBs can also be present (and enhanced) in gas with higher molecular fraction. The standard DIBs appear weak, relative to $N(\text{Na I})$, $N(\text{K I})$, and $E(B - V)$, in sight lines with appreciable molecular material at least in part because the latter trace both the atomic and the molecular gas.

Some differences in the behavior of the neutral species and DIBs may be noted in the Magellanic Clouds, where the overall metallicities and average dust-to-gas ratios are lower (by factors of ~ 2 –3 in the LMC and ~ 4 –5 in the SMC) and the typical radiation fields are somewhat stronger than in the local Galactic ISM (Lequeux 1989; Welty et al. 2012). As in our Galaxy, $N(\text{Na I})$ and $N(\text{K I})$ appear to follow nearly quadratic relationships with $N(\text{H}_{\text{tot}})$, but at much lower overall column densities – reflecting the combined effects of lower metallicities, stronger radiation fields, and (perhaps) less grain-assisted recombination (Welty & Hobbs 2001; Welty 2014; Welty & Crowther, in preparation). The relationships between $N(\text{Na I})$, $N(\text{K I})$, and $E(B - V)$ are more similar to those seen in the Galactic ISM, however, as all three of those quantities depend (to first order) on the metallicity (left-hand panel of Fig. 2). On average, the $\lambda 5780.5$, $\lambda 5797.1$, and $\lambda 6283.8$ DIBs are weaker by factors of 7–9 in the LMC and ~ 20 in the SMC, compared to Galactic sight lines with similar $N(\text{H})$ and $N(\text{H}_{\text{tot}})$ (Cox et al. 2006, 2007; Welty et al. 2006), but are only slightly weaker than for Galactic sight lines with similar $E(B - V)$ (right-hand panel of Fig. 2). While the relationship between $W(5780.5)$ and $N(\text{H})$ appears to be roughly linear in the LMC (as in our Galaxy), clear trends cannot yet be identified in the small sample available for the SMC (Welty et al. 2012; Welty 2014). In the Magellanic Clouds, the strengths of the $\lambda 5780.5$, $\lambda 5797.1$, and $\lambda 6283.8$ DIBs generally fall below the Galactic trends versus $N(\text{Na I})$ and $N(\text{K I})$ (right-hand panel of Fig. 3), with the most deficient values for both the LMC and SMC roughly a factor of 10 lower

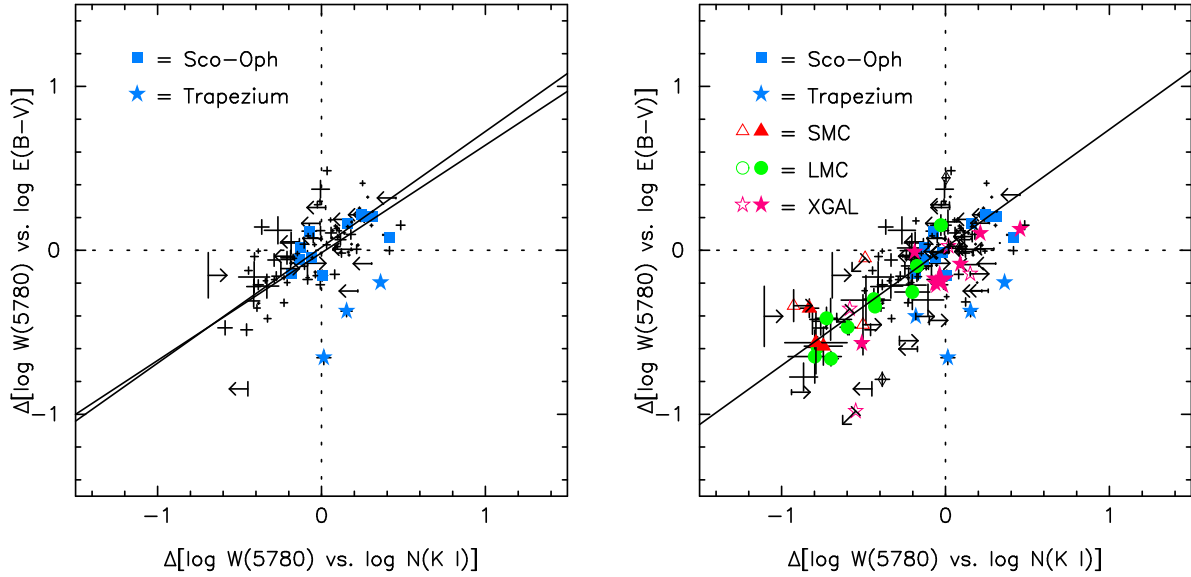


Fig. 4.— Residuals (observed minus mean relationship) for $W(5780.5)$ versus $E(B - V)$, plotted against corresponding residuals for $W(5780.5)$ versus $N(K I)$, for Galactic sight lines in the sample of Friedman et al. (2011) (left) and for an expanded sample which includes LMC, SMC, and other extragalactic (XGAL) sight lines (right). The best-fit lines, for weighted and unweighted fits to the Galactic data (excluding the Trapezium and Sco-Oph sight lines), have slopes ~ 0.7 . The observed relationship between the residuals appears to reflect the fraction of denser molecular gas; sight lines dominated by molecular material tend to have large negative residuals with respect to the general trends for $W(5780.5)$ versus both $N(K I)$ and $E(B - V)$. The LMC, SMC, and other extragalactic sight lines appear to follow a very similar trend. Given measurements of $N(K I)$ and $W(5780.5)$, this relationship can be used to refine estimates for $E(B - V)$ derived from observations of $W(5780.5)$ alone – though it does not account for the possible effects of strong local radiation fields (e.g., for the Trapezium sight lines).

than the mean Galactic values (but comparable to the lowest observed Galactic values). Even the unusual SMC sight line toward Sk 143 – where a higher than typical ratio of density to radiation field may be responsible for the observed Galactic-like abundances of the trace neutral species, CH, C₂, C₃, CN, and the C₂-DIBs – exhibits weak ”standard” DIBs (Welty et al. 2006, 2013). In the LMC and SMC, the residuals for the observed $W(5780.5)$, relative to the mean Galactic relationships versus $N(\text{K I})$ and $E(B - V)$, appear to follow the same trend seen in the local Galactic ISM (right panel of Fig. 4). While the most deficient of the Magellanic Clouds $W(5780.5)$ generally are for sight lines with stronger molecular absorption, in most cases the overall molecular fractions are not as high as those for the Galactic sight lines with weaker than expected DIBs. Additional metallicity-related effects may weaken the DIBs in the LMC and SMC.

4.2. The ISM in M82

The various absorption features observed toward SN 2014J that are due to interstellar material in M82 (Table 2) exhibit both similarities and intriguing differences, when compared to the trends found in our Galaxy and in the Magellanic Clouds. Overall, the $N(\text{K I})/N(\text{Na I})$ and $N(\text{CH})/N(\text{K I})$ ratios are quite consistent with the local Galactic values; the ”individual” component values obtained from fits to the line profiles are, in most cases, also reasonably consistent. The $N(\text{Ca I})/N(\text{K I})$ ratio is high, especially for the higher velocity components ($v_{\text{LSR}} \gtrsim 140 \text{ km s}^{-1}$) – suggestive of relatively mild depletion of calcium in M82 (Welty et al. 2003). The general decline of the $N(\text{Na I})/N(\text{Ca II})$ ratio with increasing velocity also suggests less severe depletions in the higher velocity gas (Ritchey et al. 2014b). While CN is detected, $N(\text{CN})$ falls well within the range observed for similar $N(\text{CH})$ in the local Galactic ISM; the $N(\text{CN})/N(\text{CH})$ ratio is not as high as those seen in CN-rich Galactic sight lines (e.g., toward HD62542 and HD204827). The column density of CH⁺, however, is very high; to our knowledge, the $N(\text{CH}^+)/N(\text{CH})$ ratio in the M82 components is significantly exceeded in our Galaxy only for some sight lines in the Pleiades (e.g., Ritchey et al. 2006; Fig. 5). The bulk of the M82 molecular material toward SN 2014J is thus unlikely to be in very dense clouds, and non-thermal chemical processes (needed to form the abundant CH⁺; e.g., Zsargó & Federman 2003) must be quite active.

The DIBs in M82 seen toward SN 2014J also exhibit some similarities and some differences, relative to the general trends in the local Galactic ISM. When plotted versus $N(\text{K I})$, for example, the equivalent widths of six of the ten DIBs toward SN 2014J in Table 2 ($\lambda\lambda$ 4963.9, 5487.7, 5780.5, 6196.0, 6203.6, 6283.8) are within $\pm 20\%$ of the mean Galactic values at $\log[N(\text{K I})] = 12.28$ (Fig. 3); the $\lambda 5705.1$ and $\lambda 6379.3$ DIBs are weaker by 20–45%; and the $\lambda 5797.1$ and $\lambda 6613.6$ DIBs are stronger by 25–40%. The $W(5797.1)/W(5780.5)$ ratio is thus fairly high (~ 0.7), suggestive of a relatively weak ambient radiation field and/or a somewhat shielded environment. The combination of a high $W(5797.1)/W(5780.5)$ ratio and a high $N(\text{CH}^+)/N(\text{CH})$ ratio is unusual, as those two ratios exhibit a fairly tight anti-correlation in the local Galactic ISM (Fig. 5); most of the LMC, SMC, and other extragalactic sight lines are consistent with that anti-correlation. The slight

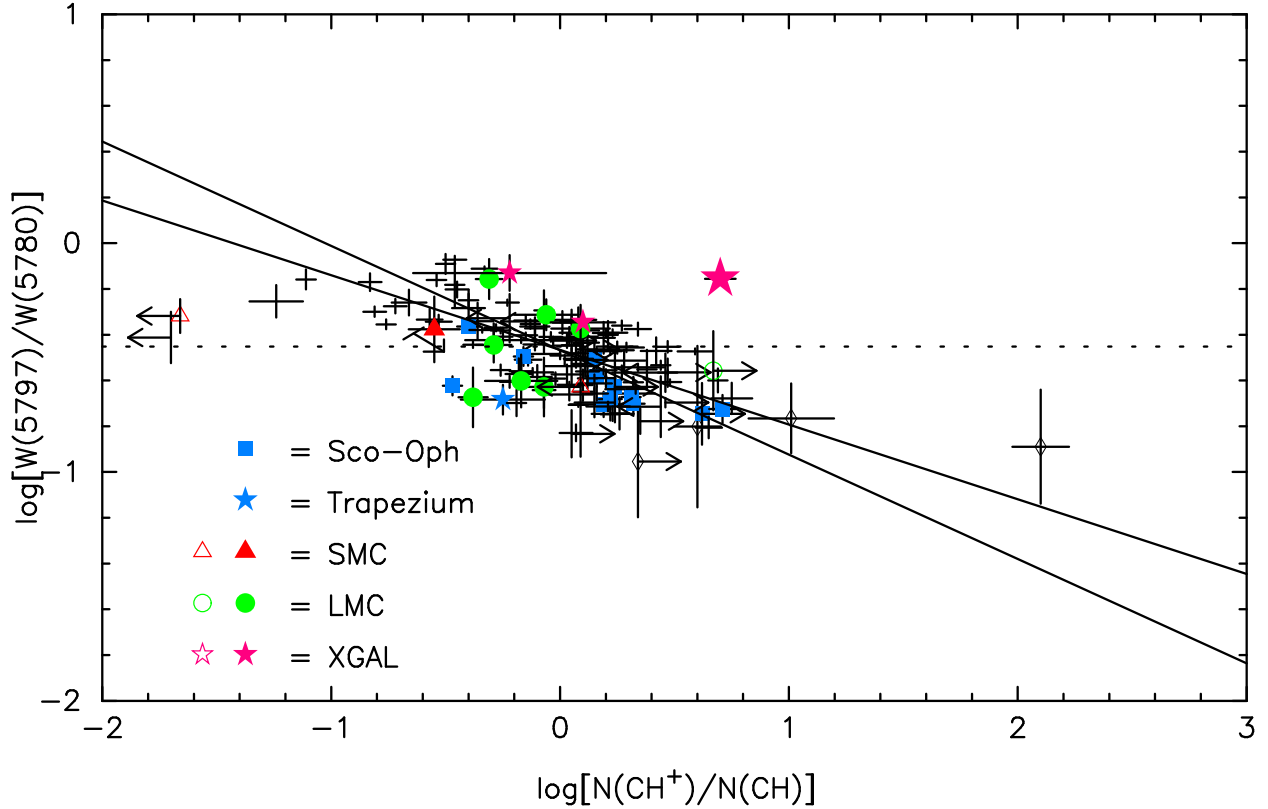


Fig. 5.— Ratio of DIB equivalent widths $W(5797.1)/W(5780.5)$ versus ratio of column densities $N(\text{CH}^+)/N(\text{CH})$. The two ratios are anti-correlated in the local Galactic ISM (though points for most sight lines in the LMC and SMC, and toward SN 1986G in NGC 5128 and SN 2008fp in ESO428-G14, also are consistent); the best-fit lines have slopes ~ -0.4 . The open black diamonds [several with large $N(\text{CH}^+)/N(\text{CH})$] represent sight lines in the Pleiades; the sight line toward SN 2014J (large red star) exhibits a unique combination of high values for both ratios.

weakness of the M82 $\lambda 5780.5$ DIB, relative to the Galactic trend with $N(\text{K I})$ (right-hand panel of Fig. 3), suggests that the sight line toward SN 2014J is not dominated by cold, dense molecular gas – consistent with indications from the molecular column densities – and also that there are no strong metallicity-related effects on the M82 DIBs (as perhaps seen for sight lines in the SMC) – consistent with the slightly sub-solar metallicity, $[\text{Fe}/\text{H}] \sim -0.35$ dex, found for the nuclear region of M82 (Origlia et al. 2004). The weakness of the $\lambda 6379.3$ DIB toward SN 2014J was immediately suggested by comparison with the adjacent $\lambda 6376.1$ DIB – the two DIBs have similar central depths toward SN 2014J (Fig. 1), whereas the $\lambda 6379.3$ DIB is typically several times deeper than the $\lambda 6376.1$ DIB in the local Galactic ISM (e.g., Galazutdinov et al. 2008b; Hobbs et al. 2008, 2009).

Of the four other extragalactic sight lines in Table 2, those toward SN 1986G, SN 2006X, and SN 2008fp were included because molecular species have been detected there. Toward both SN 2006X and SN 2008fp, the $N(\text{CN})/N(\text{CH})$ ratios are quite high and the $N(\text{CH}^+)/N(\text{CH})$ ratios are relatively low (Lauroesch et al. 2006; Patat et al. 2007; Cox & Patat 2008, 2014) – suggesting that the main host galaxy components contain relatively cold, dense gas. For SN 2008fp, analysis of the C_2 rotational excitation yields a kinetic temperature of order 30 K and a density of ”collision partners” $n_c = n(\text{H}) + n(\text{H}_2) \sim 200 \text{ cm}^{-3}$ (assuming a Galactic-like near-IR radiation field; Cox & Patat 2014); the total hydrogen density will be somewhat larger than n_c , given the apparently significant molecular fraction. The fairly high host galaxy $N(\text{Ca I})/N(\text{K I})$ ratios toward those two SNe, normally associated with milder depletions in relatively diffuse gas, are thus somewhat unexpected. As for SN 2014J, the host galaxy $N(\text{CH})/N(\text{K I})$ ratios toward the other four SNe are generally consistent with typical Galactic values.

Some differences in DIB behavior are also seen among the other extragalactic sight lines. The sight lines toward SN 1986G (NGC 5128) and SN 2001el (NGC 1448) appear to be characterized by relatively ”normal” DIB strengths versus both $N(\text{K I})$ and $E(B - V)$, except for the weak $\lambda 5797.1$ DIB toward SN 2001el (D’Odorico et al. 1989; Sollerman et al. 2005). In the CN-rich sight lines to SN 2006X (M100) and SN 2008fp (ESO428-G14), however, the DIBs generally fall well below the Galactic trends in $W(\text{DIB})$ versus $N(\text{K I})$ – similar to the DIBs toward HD62542. Of the two other SNe in the Phillips et al. (2013) sample with low $W(5780.5)$, relative to $N(\text{K I})$ and $E(B - V)$, SN 2009ig also exhibits strong CN absorption (Cox & Patat 2014), while no information is available for the molecular absorption toward SN 2009le. The $\lambda 6379.3$ DIB is weaker than the $\lambda 6196.0$ DIB toward both SN 2006X and SN 2008fp, and is only slightly deeper than the $\lambda 6376.1$ DIB toward SN 2008fp.

4.3. Shifted DIBs in M82

One other notable difference in the behavior of the M82 DIBs is that the profiles of many of the DIBs appear to be shifted in velocity, relative to the envelope of the K I $\lambda\lambda 7664, 7698$ profiles toward SN 2014J, with different shifts for different DIBs. For example, while the $\lambda 4963.9$ DIB is

fairly well aligned with the strongest K I (and CH) absorption, the $\lambda\lambda 5780.5$, 5797.1 , and 6613.6 DIBs are shifted to the red (Fig. 6). In the Galactic ISM, the equivalent widths of the DIBs are generally correlated with $N(\text{K I})$, with the narrower DIBs exhibiting the best correlations (Fig. 3; Herbig 1993; Krelowski et al. 1998; Welty 2014). The rest wavelengths adopted for the DIBs have therefore often been estimated via comparisons with the profiles of the K I lines in relatively simple sight lines. Combined contributions from the various components discernible in high-resolution spectra of Na I and/or K I for more complex sight lines can thus produce apparent shifts in the broader, unresolved DIB profiles – e.g., for HD183143 versus HD204827 (Hobbs et al. 2008, 2009) or (perhaps) for some sight lines in Sco OB1 (Galazutdinov et al. 2008a) – though not all observed DIB shifts can be explained in that way (e.g., for Herschel 36; Dahlstrom et al. 2013).

We have attempted to model the M82 DIB profiles toward SN 2014J by combining “intrinsic” DIB profiles for all the velocity components seen in K I toward the SN. The intrinsic DIB profiles, expressed as apparent optical depths as functions of velocity, were derived from ARCES spectra of 20 Aql, which has a single strong K I component (at ARCES resolution) and fairly narrow observed DIBs. Weighting the components according to their K I column densities and scaling the combined profiles to the observed central depths of the DIBs yields the profiles shown in red in Figure 6, which do not match the observed DIB profiles (except for $\lambda 4963.9$). Weighting the weaker, higher velocity K I components more heavily, however, can yield combined profiles that match the observed profiles fairly well. For example, the green lines in Figure 6 show the model profiles obtained by giving higher weight to the weaker K I components – by factors of 2 for $\lambda 4963.9$, 3 for $\lambda 5797.1$ and $\lambda 6196.0$, and 7 for $\lambda 5780.5$ and $\lambda 6613.6$. Changing those weighting factors for the weaker K I components by ± 1 generally yields somewhat poorer fits to the DIB profiles. That simple bi-modal weighting of the two groups of K I components appears to yield reasonably good matches to the observed profiles – except for the narrow $\lambda 6196.0$ DIB, for which a more complex weighting scheme may be needed. The “extra” absorption near $v_{\text{LSR}} = 0 \text{ km s}^{-1}$ for the $\lambda\lambda 5780.5$, 5797.1 , and 6613.6 DIBs is likely Galactic (which was not included in the model profiles). The factor-of-7 range in individual component $W(5780.5)/N(\text{K I})$ implied by the differences in weighting is not unreasonable, given the observed range in total sight line values in the right-hand panel of Figure 3.

The differences in weighting of the stronger main and weaker, higher velocity K I components needed to fit the observed DIB profiles suggest that the two groups of components/clouds are characterized by different physical/environmental conditions and provide some indications as to how the different DIBs respond to those conditions. Given the relative weights 1:3 and 1:7 noted above for the $\lambda 5797.1$ and $\lambda 5780.5$ DIBs and the column densities of K I in the main and higher velocity component groups (14.4 and $4.4 \times 10^{11} \text{ cm}^{-2}$, respectively), we can estimate the equivalent widths of the two DIBs in the two component groups: 110 and 100 m\AA for $\lambda 5797.1$ and 102 and 217 m\AA for $\lambda 5780.5$. For atomic hydrogen, the Galactic relationship $\log[N(\text{H})] = 19.05 + 0.92 \times \log[W(5780.5)]$ (e.g., Friedman et al. 2011) and those $\lambda 5780.5$ equivalent widths would imply $\log[N(\text{H})] \sim 20.90$ and 21.20 cm^{-2} , respectively. Similarly, the observed $N(\text{CH})$ in the two component groups (4.0 and $0.3 \times 10^{13} \text{ cm}^{-2}$) would imply $\log[N(\text{H}_2)] \sim 21.03$ and 19.89 cm^{-2} ,

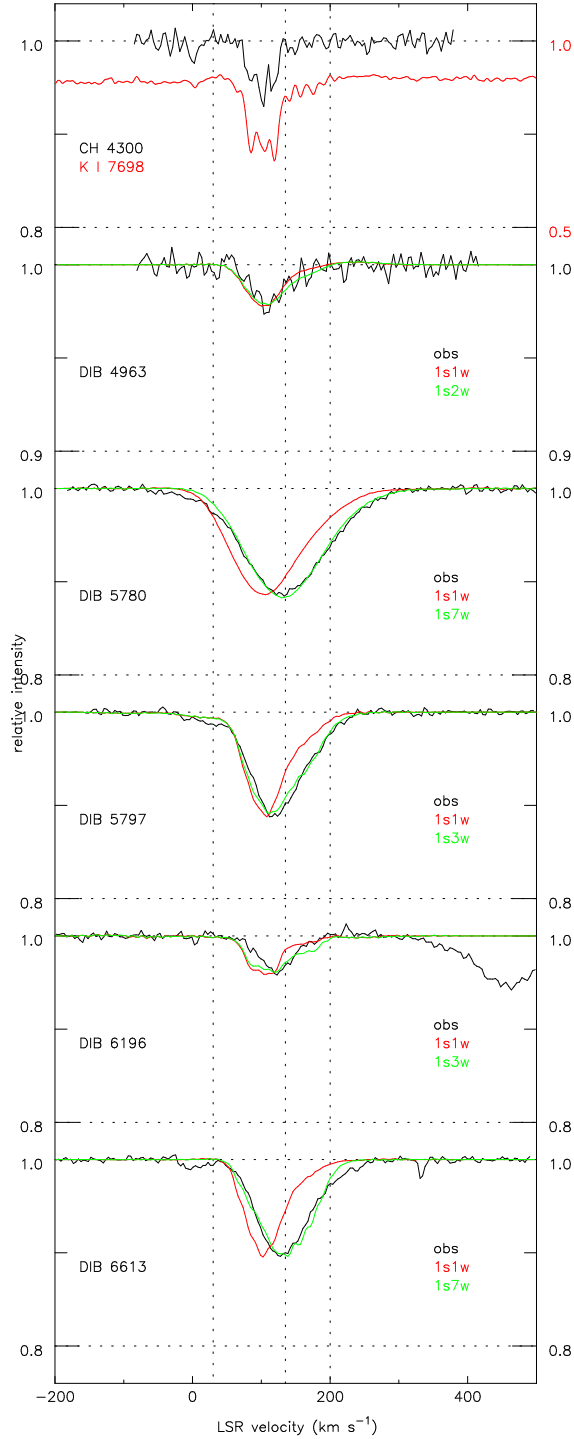


Fig. 6.— Profiles of K I $\lambda 7698$, CH $\lambda 4300$, and five DIBs toward SN 2014J. The vertical dotted lines separate the three groups of components seen in K I: Galactic; main M82; and weaker, higher velocity M82. Note the apparent offsets in velocity between K I/CH and the $\lambda\lambda 5780.5$, 5797.1 , 6196.0 , and 6613.6 DIBs. For the DIBs, the black line shows the observed profile; the red line shows the model profile based on weighting the K I components by $N(\text{K I})$ alone (using “intrinsic” DIB profiles from ARCES spectra of 20 Aql); and the green line shows the model profile where the weaker, higher velocity K I components are weighted more heavily (by factors of 2 for $\lambda 4963.9$, 3 for $\lambda 5797.1$ and $\lambda 6196.0$, and 7 for $\lambda 5780.5$ and $\lambda 6613.6$). Residuals near $v_{\text{LSR}} = 0 \text{ km s}^{-1}$ for several of the DIBs represent contributions from the Galactic ISM.

respectively (for $\log[N(\text{H}_2)] = 6.82 + 1.045 \times \log[N(\text{CH})]$, as seen in our Galaxy and in the LMC; e.g., Welty et al. 2006). The main K I component group would thus contain about 65% of the total hydrogen in the sight line, with molecular fraction $f(\text{H}_2) \sim 0.7$. The weaker, higher velocity K I component group would have about 70% of the atomic hydrogen, with much lower $f(\text{H}_2) \sim 0.1$. As discussed by Ritchey et al. (2014b), the 21 cm emission in the direction of the SN (M. Yun 2014, private communication) peaks between about 100 and 160 km s⁻¹; slightly more than half the M82 emission is over the velocity range corresponding to the weaker K I components.

In principle, several additional factors could affect these estimates for the atomic and molecular content in the two M82 component groups. First, the $N(\text{H})$ predicted from $W(5780.5)$ could be slightly underestimated if the metallicity of M82 is slightly sub-solar (Origlia et al. 2004). Even factor-of-2 increases in $N(\text{H})$, however, would not alter the characterization of the two component groups as significantly molecular and primarily atomic, respectively. Second, the high CH^+ abundance toward SN 2014J might signal that the normal relationship between CH and H_2 may not apply – as CH can be produced non-thermally along with CH^+ (e.g., Zsargó & Federman 2003) and as there are Galactic sight lines with enhanced CH^+ and lower than average $N(\text{H}_2)/N(\text{CH})$ ratios [e.g., 23 Ori (Welty et al. 1999); Herschel 36 (Dahlstrom et al. 2013)]. While the true column densities of H_2 (and the corresponding molecular fractions) could thus be lower, we note that the $N(\text{CN})/N(\text{CH})$ ratio toward the SN is much higher than toward 23 Ori or Herschel 36 – suggesting that at least a significant fraction of the CH seen toward the SN is due to equilibrium chemistry.

For the DIBs, the heavier weighting of the weaker K I components for the $\lambda 5780.5$ DIB, relative to the $\lambda 5797.1$ DIB, implies that $W(5797.1)/W(5780.5) \sim 0.46$ in those weaker, predominantly atomic components, suggestive of reduced shielding and/or stronger ambient radiation fields there. In the stronger K I components, where $f(\text{H}_2)$ is higher, the implied $W(5797.1)/W(5780.5) \sim 1.1$, which is comparable to the highest values measured for that ratio (e.g., Vos et al. 2011). The $\lambda 5780.5$ DIB is weak, relative to $N(\text{K I})$, in the main M82 components, but is consistent with the mean Galactic trend in the weaker, higher velocity components. The heavier relative weighting of the stronger K I components (where CH is more abundant) for the $\lambda 4963.9$ C₂-DIB, compared to the relative weighting for the $\lambda 5780.5$ DIB, is consistent with the picture that the C₂-DIBs trace gas with higher molecular fractions, while the broader "standard" DIBs trace primarily atomic gas. A similar situation may be present toward SN 2008fp (ESO428-G14), where the weaker than "expected" $\lambda 5780.5$ DIB appears to be slightly offset from the strongest component seen in CN and K I (Phillips et al. 2013; Cox & Patat 2014).

4.4. Predicting $N(\text{H})$ and $E(B - V)$

Given the relationships found between the DIBs and various other constituents of the ISM in our Galaxy and in the Magellanic Clouds, it is of interest to see whether observations of the DIBs can be used to estimate $N(\text{H})$ and $E(B - V)$ when direct measurements of those quantities are not available or feasible. For example, the generally good, nearly linear correlation between

$W(5780.5)$ and $N(\text{H})$ in the Galactic ISM ($r = 0.90$; slope ~ 1.05 ; Friedman et al. 2011; Welty 2014) suggests that reasonable estimates for $N(\text{H})$ might be obtained from measurements of the $\lambda 5780.5$ DIB, both for sight lines where UV spectra of Lyman- α absorption are not available (e.g., toward SN 2014J, as in Sec. 4.3 above) and toward stars of spectral type later than about B3 (where stellar Lyman- α absorption becomes strong). The estimated $N(\text{H})$ could be too small, however, for sight lines characterized by strong radiation fields (as in the Orion Trapezium region) or by significantly sub-solar metallicities (as in the LMC and SMC), where the DIBs can be significantly weaker. While estimates for $E(B - V)$ based on the Galactic relationships with the DIB equivalent widths should not be as significantly affected by differences in metallicity, the "standard" DIBs can be weaker than expected – and $E(B - V)$ thus underestimated – when the molecular fraction is large. Examination of the DIB equivalent widths versus $N(\text{K I})$ and/or $N(\text{Na I})$ [and of the $N(\text{CN})/N(\text{CH})$ ratio, when available] may aid in identifying such cases – and may also enable some refinement of the estimated $E(B - V)$.

In light of the use of Type Ia SNe as "standard candles" for investigations of the expansion of the Universe and of the potential effects of intervening dust on the brightness and colors of those SNe, independent estimates for the host galaxy extinction would be valuable. Phillips et al. (2013) compared host galaxy visual extinctions A_V , derived from optical and near-IR photometry, with host galaxy $N(\text{Na I})$ toward 32 extragalactic Type Ia SNe; they also determined $N(\text{K I})$ and/or $W(5780.5)$ for roughly one-third of the sample. Phillips et al. found that where the $\lambda 5780.5$ DIB is detected, predictions of A_V based on $W(5780.5)$ are more consistent with the adopted host galaxy A_V than are the corresponding predictions from either the equivalent widths of the Na I D-lines ($\lambda\lambda 5890.0, 5895.9$) or $N(\text{Na I})$. [While in principle A_V should be a better indicator of the total amount of dust, we use $E(B - V)$ here, because there are more extensive Galactic data for $E(B - V)$ and because (curiously) the DIBs appear to be somewhat better correlated with $E(B - V)$ than with A_V .] For the six SNe with detections of both K I and the $\lambda 5780.5$ DIB in the Phillips et al. sample, the ratios of the $E(B - V)$ predicted from $W(5780.5)$ to the $E(B - V)$ derived from photometry of the SN range from 0.27 to 1.38. If the predicted $E(B - V)$ are adjusted based on the relationship between the residuals with respect to the mean Galactic trends in $W(5780.5)$ versus $N(\text{K I})$ and $E(B - V)$ (Fig. 4), then those "corrected" $E(B - V)$ are in better agreement with the adopted $E(B - V)$ for four of the six SNe, and the predicted/adopted ratios range from 0.59 to 1.36.

As the equivalent widths of other DIBs also appear to be reasonably well correlated with $E(B - V)$ (e.g., Friedman et al. 2011; Welty 2014; see also Appendix Table 3), similar estimates for $E(B - V)$ may be derived from measurements of those other DIBs. Column 9 of Table 1 lists such estimates for the M82 $E(B - V)$ toward SN 2014J, derived from the equivalent widths of the ten DIBs considered in this paper. As noted above, comparisons of the M82 DIB equivalent widths and $N(\text{K I})$ with the Galactic trends for $W(\text{DIB})$ versus $N(\text{K I})$ suggest that some DIBs ($\lambda\lambda 5705.1, 6379.3$) will yield underestimates for $E(B - V)$, while several others ($\lambda\lambda 5797.1, 6613.6$) will yield overestimates. The values of $E(B - V)$ estimated from the ten DIBs range from 0.43 to

1.18; the mean \pm standard deviation is 0.78 ± 0.24 . Adjustment of the various estimated $E(B - V)$ for the residuals seen in $W(\text{DIB})$ versus $N(\text{K I})$ narrows the range from 0.59 to 0.96, with mean \pm standard deviation 0.75 ± 0.12 (column 10 of Table 1) – consistent with the value $\sim 0.65 \pm 0.30$ that would be predicted for the observed $N(\text{K I})$. Within the mutual uncertainties, these estimates for the host galaxy reddening are consistent with the low end of the range in $E(B - V)$ derived from optical and near-IR photometry of the SN (Polshaw et al. 2014; c.f. Goobar et al. 2014).

5. SUMMARY / CONCLUSIONS

We have discussed the interstellar absorption features found in moderately high resolution, high S/N ratio optical spectra of SN 2014J (in the nearby galaxy M82), obtained with the ARC echelle spectrograph at Apache Point Observatory between 2014 January 27 and March 04 (bracketing the maximum V-band brightness of the SN). Complex absorption from Na I, K I, Ca I, and Ca II is seen for LSR velocities between about -53 and $+257$ km s $^{-1}$. The absorption at $v_{\text{LSR}} \lesssim 30$ km s $^{-1}$ is due to gas in the Galactic disk and halo; the absorption at higher velocities arises in gas associated with M82. Absorption from CH, CH $^+$, and/or CN is seen for the strongest M82 components between 80 and 120 km s $^{-1}$. Many of the diffuse interstellar bands are also detected, at velocities corresponding to gas in M82.

Comparisons of the interstellar absorption in M82 with trends seen in the local Galactic ISM, in the lower metallicity Magellanic Clouds, and in other galaxies probed by SNe reveal both similarities and some intriguing differences. Overall, the $N(\text{K I})/N(\text{Na I})$ and $N(\text{CH})/N(\text{K I})$ ratios are very similar to those seen in our Galaxy; $N(\text{CN})$ is also quite consistent with the values seen locally, for comparable $N(\text{CH})$. The $N(\text{Ca I})/N(\text{K I})$ ratio is high, suggestive of relatively mild depletion of calcium in M82, particularly in the higher velocity components. The $N(\text{CH}^+)/N(\text{CH})$ ratio is very high – significantly exceeded in the Galactic ISM only in several sight lines in the Pleiades. The moderate $N(\text{CN})/N(\text{CH})$ and very high $N(\text{CH}^+)/N(\text{CH})$ suggest that the molecular material toward SN 2014J is unlikely to be in very cold, dense clouds. Of the ten DIBs considered in this paper, six ($\lambda\lambda 4963.9, 5487.7, 5780.5, 6196.0, 6203.6, 6283.8$) have equivalent widths within $\pm 20\%$ of the mean Galactic values for the observed $N(\text{K I})$; $\lambda 5705.1$ and $\lambda 6379.3$ are weaker by 20–45%; and $\lambda 5797.1$ and $\lambda 6613.6$ are stronger by 25–40%. The overall $W(5797.1)/W(5780.5)$ ratio is thus fairly high (~ 0.7) – suggestive of relatively weak ambient radiation fields and/or shielded environments. The combination of a high $N(\text{CH}^+)/N(\text{CH})$ ratio and a high $W(5797.1)/W(5780.5)$ ratio is very unusual, as those two ratios exhibit a fairly tight anticorrelation in the Galactic ISM (and elsewhere).

While $W(5780.5)$ is moderately correlated with both $N(\text{K I})$ ($r \sim 0.71$) and $E(B - V)$ ($r \sim 0.82$) in the Galactic ISM, the DIB is weaker than expected, relative to $N(\text{K I})$ and/or $E(B - V)$, in a number of Galactic and extragalactic sight lines; the residuals (with respect to the mean Galactic trends) for $W(5780.5)$ versus $N(\text{K I})$ and $W(5780.5)$ versus $E(B - V)$ are correlated. In general, the sight lines in which the $\lambda 5780.5$ DIB appears to be weak also exhibit fairly high $N(\text{CN})$ and/or

fairly high molecular fractions $f(\text{H}_2)$. Similar behavior is exhibited by the other "standard" DIBs considered in this paper – particularly the broader DIBs. Those DIBs appear weak, relative to $N(\text{K I})$ and/or $E(B - V)$, in sight lines with significant molecular fractions, at least in part because they trace primarily atomic gas, whereas K I and $E(B - V)$ trace both atomic and molecular material. The $\lambda 4963.9$ "C₂-DIB" is not weaker than expected in those sight lines, however, because the C₂-DIBs can be present (and enhanced) in molecular gas.

The profiles of many of the M82 DIBs appear to be shifted in velocity, relative to the envelope of the K I profiles toward SN 2014J, with different shifts for different DIBs. The DIB profiles toward SN 2014J may be modeled by combining "intrinsic" DIB profiles (derived from ARCES spectra of 20 Aql) for all the velocity components seen in K I . Uniform weighting of the K I components by $N(\text{K I})$ yields a good match to the observed DIB profile only for the $\lambda 4963.9$ C₂-DIB; heavier relative weighting of the weaker, higher velocity K I components is required to fit the observed profiles of the other "standard" DIBs – e.g., by factors of about 3 for the $\lambda 5797.1$ DIB and about 7 for the $\lambda 5780.5$ DIB. The differences in relative weighting [i.e., in $W(\text{DIB})/N(\text{K I})$] are suggestive of differences in local physical/environmental conditions in the stronger "main" M82 components and in the weaker, higher velocity components – and of differences in the responses of the various DIBs to those local conditions. If standard Galactic relationships between $W(5780.5)$ and $N(\text{H})$ and between $N(\text{CH})$ and $N(\text{H}_2)$ are used to predict $N(\text{H})$ and $N(\text{H}_2)$ in those two component groups, we estimate that the stronger main components would contain about 65% of the total hydrogen in the sight line, with $f(\text{H}_2) \sim 0.7$ and $W(5797.1)/W(5780.5) \sim 1.1$ and the weaker, higher velocity components would contain about 70% of the total atomic hydrogen, with $f(\text{H}_2) \sim 0.1$ and $W(5797.1)/W(5780.5) \sim 0.46$. The $\lambda 4963.9$ C₂-DIB and (to a lesser degree) the $\lambda 5797.1$ DIB are stronger in the main, largely molecular components, while the $\lambda 5780.5$ and $\lambda 6613.6$ "standard" DIBs are stronger in the higher velocity, primarily atomic components.

The correlation between the residuals, relative to the mean Galactic trends, of $W(5780.5)$ versus $N(\text{K I})$ and $W(5780.5)$ versus $E(B - V)$ suggests that comparisons of $W(5780.5)$ with $N(\text{K I})$ may be used to identify cases where estimates of $E(B - V)$ based on the measured $W(5780.5)$ would be too small – and then to refine those estimates for $E(B - V)$. Application of such a procedure yields better agreement between the host galaxy $E(B - V)$ estimated from $W(5780.5)$ and the values derived from optical and near-IR photometry for several of the SNe in the sample of Phillips et al. (2013). Estimates of the reddening due to dust in M82 along the sight line to SN 2014J, derived from the equivalent widths of the ten DIBs considered in this paper, yield $E(B - V) \sim 0.75 \pm 0.12$ mag – consistent with the value estimated from $N(\text{K I})$ and with the lower end of the values obtained from photometry of the SN.

Support for this work has been provided by the National Science Foundation, under grants AST-1009603 (DGY), AST-1008424 (JD), and AST-1238926 (DEW). AR gratefully acknowledges support from the Kennilworth Fund of the New York Community Trust.

Facilities: ARC (ARCES)

REFERENCES

- Ádámkóvics, M., Blake, G. A., & McCall, B. J. 2005, *ApJ*, 625, 857
- Cordiner, M. A., Cox, N. L. J., Evans, C. J. et al. 2011, *ApJ*, 726, 39
- Cordiner, M. A., Cox, N. L. J., Trundle, C. et al. 2008a, *A&A*, 480, L13
- Cordiner, M. A., Smith, K. T., Cox, N. L. J. et al. 2008b, *A&A*, 492, L5
- Cox, N. L. J., Davis, P., Patat, F., & Van Winckel, H. 2014, *ATel#5797*
- Cox, N. L. J., Kaper, L., Foing, B. H., & Ehrenfreund, P. 2005, *A&A*, 438, 187
- Cox, N. L. J., & Patat, F. 2008, *A&A*, 485, L9
- Cox, N. L. J., & Patat, F. 2014, *A&A*, in press (arXiv:1403.4386)
- Cox, N. L. J., Cordiner, M. A., Cami, J. et al. 2006, *A&A*, 447, 991
- Cox, N. L. J., Cordiner, M. A., Ehrenfreund, P. et al. 2007, *A&A*, 470, 941
- Dahlstrom, J., York, D. G., Welty, D. E. et al. 2013, *ApJ*, 773, 41
- D’Odorico, S., di Serego Alighieri, S., Pettini, M. et al. 1989, *A&A*, 215, 21
- Ehrenfreund, P., Cami, J., Jiménez-Vicente, J. et al. 2002, *ApJ*, 576, L117
- Ellison, S. L., York, B. A., Murphy, M. T. et al. 2008, *MNRAS*, 383, L30
- Foley, R. J., & Kirshner, R. P. 2013, *ApJ*, 769, L1
- Fossey, S. J. et al. 2014, *CBET*, 3792
- Friedman, S. D., York, D. G., McCall, B. J. et al. 2011, *ApJ*, 727, 33
- Galazutdinov, G. A., Lo Curto, G., Han, I., & Krelowski, J. 2008a, *PASP*, 120, 178
- Galazutdinov, G. A., Lo Curto, G., & Krelowski, J. 2008b, *MNRAS*, 386, 2003
- Goobar, A., Johansson, J., Amanullah, R. et al. 2014, *ApJ*, 784, L12
- Herbig, G. H. 1993, *ApJ*, 407, 142
- Hobbs, L. M., York, D. G., Snow, T. P. et al. 2008, *ApJ*, 680, 1256
- Hobbs, L. M., York, D. G., Thorburn, J. A. et al. 2009, *ApJ*, 705, 32
- Kalberla, P. M. W., Burton, W. B., Hartmann, D. et al. 2005, *A&A*, 440, 775
- Krelowski, J., Galazutdinov, G. A., & Musaev, F. A. 1998, *ApJ*, 493, 217
- Lauroesch, J. T., Crotts, A. P. S., Meiring, J. et al. 2006, *CBET*, 421, 1
- Lawton, B., Churchill, C. W., York, B. A. et al. 2008, *AJ*, 139, 994
- Lequeux, J. 1989, in *Recent Developments of Magellanic Cloud Research*, ed. K. S. de Boer, F. Spite, & G. Stasińska (Paris: Obs. Paris), 119
- Origlia, L., Ranalli, P., Comastri, A., & Maiolino, R. 2004, *ApJ*, 606, 862
- Pak, S., Jaffe, D. T., van Dishoeck, E. F., Johansson, L. E. B., & Booth, R. S. 1998, *ApJ*, 498, 735

- Patat, F., Chandra, P., Chevalier, R. et al. 2007, *Science*, 317, 924
- Phillips, M. M., Simon, J. D., Morrell, N. et al. 2013, *ApJ*, 779, 38
- Polshaw, J., Kotak, R., Maund, J. R. et al. 2014, *ATel#5816*
- Ritchey, A. M., Martinez, M., Pan, K., Federman, S. R., & Lambert, D. L. 2006, *ApJ*, 649, 788
- Ritchey, A. M., & Wallerstein, G. 2012, *ApJ*, 748, L11
- Ritchey, A. M., Welty, D. E., Dahlstrom, J. A., & York, D. G. 2014a, *ATel#5859*
- Ritchey, A. M. et al. 2014b, *ApJ*, submitted
- Sheffer, Y., Rogers, M., Federman, S. R. et al. 2008, *ApJ*, 687, 1075
- Snow, T. P., Welty, D. E., Thorburn, J. et al. 2002, *ApJ*, 573, 670
- Sollerman, L., Cox, N., Mattila, S. et al. 2005, *A&A*, 429, 559
- Sternberg, A., Gal-Yam, A., Simon, J. D. et al. 2011, *Science*, 333, 856
- Sternberg, A., Gal-Yam, A., Simon, J. D. et al. 2013, *MNRAS*, submitted (arXiv:1311.3645)
- Thorburn, J. A., Hobbs, L. M., McCall, B. J. et al. 2003, *ApJ*, 584, 339
- van Loon, J. T., Bailey, M., Tatton, B. L. et al. 2013, *A&A*, 550, A108
- Vladilo, G., Crivellari, L., Molaro, P., & Beckman, J. E. 1987, *A&A*, 182, L59
- Vos, D. A. I., Cox, N. L. J., Kaper, L., Spaans, M., & Ehrenfreund, P. 2011, *A&A*, 533A, 129
- Wang, S., Hildebrand, R. H., Hobbs, L. M. et al. 2003, *Proc. SPIE*, 4841, 1145
- Welsh, B. Y., Lallement, R., Vergely, J.-L., & Raimond, S. 2010, *A&A*, 510, 54
- Welty, D. E. 2014, in *IAU Symp. 297, The Diffuse Interstellar Bands*, ed. J. Cami & N. L. J. Cox (Cambridge: Cambridge Univ. Press), 153
- Welty, D. E., Federman, S. R., Gredel, R., Thorburn, J. A., & Lambert, D. L. 2006, *ApJS*, 165, 138
- Welty, D. E., & Hobbs, L. M. 2001, *ApJS*, 133, 345
- Welty, D. E., Hobbs, L. M., & Morton, D. C. 2003, *ApJS*, 147, 61
- Welty, D. E., Howk, J. C., Lehner, N., & Black, J. H. 2013, *MNRAS*, 428, 1107
- Welty, D. E., Xue, R., & Wong, T. 2012, *ApJ*, 745, 173
- Welty, D. E., Hobbs, L. M., Lauroesch, J. T. et al. 1999, *ApJS*, 124, 465
- Wolfire, M. G., Hollenbach, D., McKee, C. F., Tielens, A. G. G. M., & Bakes, E. L. O. 1995, *ApJ*, 443, 152
- York, B. A., Ellison, S. L., Lawton, B. et al. 2006, *ApJ*, 647, L29
- York, D. G. et al. 2014, *ApJ*, submitted
- Zheng, W., Shivvers, I., Filippenko, A. V. et al. 2014, *ApJ*, 783, L24

Zsargó, J., & Federman, S. R. 2003, ApJ, 589, 319

A. Correlation Fits

Friedman et al. (2011) investigated correlations between eight DIBs and $N(\text{H})$, $N(\text{H}_2)$, and $E(B - V)$, for a sample of 133 Galactic sight lines observed with ARCES and listed coefficients found for linear fits to both $\log[N(\text{H})]$ versus $\log[W(\text{DIB})]$ and $E(B - V)$ versus $W(\text{DIB})$. We have performed similar comparisons of $\log[W(\text{DIB})]$ versus both $\log[E(B - V)]$ and $\log[N(\text{K I})]$, using both the Friedman et al. sample and a somewhat larger sample of Galactic data now available. The fit coefficients listed in columns 3–4 and 5–6 of Table 3 are the means of the values obtained for weighted and unweighted fits to the data (e.g., Welty & Hobbs 2001); in general, the various “discrepant” sight lines (Sco-Oph, Trapezium, and all extragalactic) are not included in the fits. The notes to Table 1 indicate which relationships were used to predict the Galactic and M82 DIB strengths from the respective $N(\text{K I})$ and to predict the M82 $E(B - V)$ from the DIB equivalent widths. The last four columns of Table 3 describe the correlations found between the residuals (observed minus mean) of the DIBs versus $E(B - V)$ and $N(\text{K I})$, which were used to refine the estimates for $E(B - V)$. As noted in the text, stronger correlations between the residuals (higher r values) are found for the broader DIBs.

Table 3. Correlation Fit Coefficients

DIB (1)	FWHM (Å) (2)	$E(B - V)^a$		$N(K I)^a$		Residual Plots ^b			
		a (3)	b (4)	a (5)	b (6)	r (7)	rms (8)	a (9)	b (10)
4963.9	0.62	1.465	1.140	-7.200	0.695	0.551	0.11	0.050	0.920
5487.7	5.20	2.090	0.895	-3.105	0.405	0.738	0.10	-0.040	0.755
5705.1	2.58	2.055	0.815	-3.165	0.415	0.755	0.09	0.000	0.750
5780.5	2.11	2.690	0.935	-3.355	0.480	0.683	0.10	0.000	0.690
5797.1	0.77	2.290	0.985	-4.760	0.565	0.454	0.12	0.045	0.625
6196.0	0.42	1.735	0.945	-4.785	0.520	0.580	0.10	0.010	0.625
6203.6	4.87	2.295	0.885	-2.985	0.415	0.726	0.10	-0.010	0.720
6283.8	4.77	3.085	0.820	-1.835	0.390	0.754	0.11	0.005	0.665
6379.3	0.58	1.940	0.960	-6.555	0.685	(0.00)	(0.70)
6613.6	0.93	2.380	1.195	-6.535	0.715	0.489	0.14	0.030	0.545

^aRelations are $\log[W(\text{DIB})] = a + b \times \log[x]$, where $x = E(B - V)$ or $N(K I)$.

^bResiduals are observed $\log[W(\text{DIB})]$ minus value for mean Galactic relationship. Fits are to residual with respect to $\log[E(B - V)]$ versus residual with respect to $\log[N(K I)]$. The linear correlation coefficient (r) and rms deviation of the residuals vs. the fit are also given. Representative values for the slope and intercept were used for the $\lambda 6379.3$ DIB.